

**HETEROGENEOUS CATALYTIC OXIDATION  
OF METHYLENE BLUE BY AMINE-  
FUNCTIONALIZED TITANIUM-  
TEREPHTHALATE METAL ORGANIC  
FRAMEWORK, NH<sub>2</sub>-MIL-125(Ti)**

**TEO SZE A ERR**



**THESIS SUBMITTED IN FULFILLMENT FOR  
THE DEGREE OF MASTER OF SCIENCE**

**FACULTY OF SCIENCE AND NATURAL  
RESOURCES  
UNIVERSITI MALAYSIA SABAH  
2017**

## DECLARATION

I hereby declare that the material in this thesis is my own except for quotations, excerpts, equations, summaries and references, which have been duly acknowledged.

08 August 2017

---

TEO SZIA ERR

MS1421118T



UMMS  
UNIVERSITI MALAYSIA SABAH

## CERTIFICATION

NAME : **TEO SZEA ERR**  
MATRIC NO. : **MS1421118T**  
TITLE : **HETEROGENEOUS CATALYTIC OXIDATION OF METHYLENE  
BLUE BY AMINE-FUNCTIONALIZED TITANIUM-  
TEREPHTHALATE METAL ORGANIC FRAMEWORK, NH<sub>2</sub>-MIL-  
125(Ti)**  
DEGREE : **MASTER OF SCIENCE  
(INDUSTRIAL CHEMISTRY)**  
VIVA DATE : **17 JULY 2017**



**CERTIFIED BY**  
**UMMS**  
SIGNATURE  
UNIVERSITI MALAYSIA SABAH

---

## **ACKNOWLEDGEMENTS**

First and foremost, I would like to express my thanks and respect for my supervisor and mentor, Dr Moh Pak Yan. He was always looking out for me, showed me respect and treated me as equals.

I would also like to acknowledge University Malaysia Sabah for providing me with the facilities to conduct my research. To the lab staff, Mr. Abdul Rahim Bin Ahmad, Mr. Jerry Alexander, Mr. Recheidy and Mr. Taipin for their expertise and technical support.

I would like to express my gratitude to MyBrain15 and Exploratory Research Grant Scheme (ERGS) for financial support.

I would like to thank God Almighty, for without His countless graces and blessings, this thesis would not have been completed.

I would like to thank my family for their unrelenting support.

My mum, with her never-ending support of my pursue of knowledge.

My cousin and friend, Yuan, for always being there during my busiest of moments. If it were not for you, my work would have been completed much earlier.

My best friend, Shane, sticking with me through every highs and lows, ups and downs, good and bad.

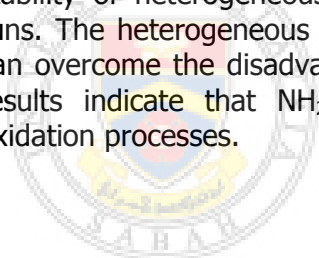
And finally, my esteemed colleagues. Von Fei, my comrade in arms through every step, leap and milestone. Yang, my Santa Claus, giving me what I need when I needed it the most. And Wai Hung, for simply being there.

Teo Szea Err

21 August 2017

## ABSTRACT

Iron oxide sludge formation, high pH dependency, and poor catalyst reusability have always been critical drawbacks of Fenton's reagent. In this work, titanium-terephthalate metal organic framework, NH<sub>2</sub>-MIL-125(Ti), was proposed as heterogeneous Fenton-like catalyst for methylene blue degradation. NH<sub>2</sub>-MIL-125(Ti) is a metal-organic compound possessing high surface area, photocatalytic properties and unique dual-porosity. MIL-125(Ti) and NH<sub>2</sub>-MIL-125(Ti) was prepared through reflux method and activated using conventional solvent exchange method. Both samples were confirmed by XRD and FTIR. SEM images showed that NH<sub>2</sub>-MIL-125(Ti) has spherical morphology with size ranging from 250 to 500 nm which is at least half of the size of MIL-125(Ti). NH<sub>2</sub>-MIL-125(Ti) is stable under water with superior adsorption and photocatalytic activities upon visible and UV-A irradiation. Furthermore, the results revealed that NH<sub>2</sub>-MIL-125(Ti) is an effective non-ferrous Fenton-like catalyst. Synergistic effect was observed between NH<sub>2</sub>-MIL-125(Ti) and H<sub>2</sub>O<sub>2</sub>, with 84 % of removal efficiency in 40 ppm of methylene blue. Results showed that •OH and h<sup>+</sup> are the dominant species in Fenton-like oxidation of NH<sub>2</sub>-MIL-125(Ti)/H<sub>2</sub>O<sub>2</sub> catalytic system. Photoenhancement was proven to be effective where up to 92 % removal was obtained when exposed to UV-A light. NH<sub>2</sub>-MIL-125(Ti) showed low pH dependency with stable degradation from pH 3 to 9. Negligible amount of titanium leaching was detected which indicates the high stability of heterogeneous NH<sub>2</sub>-MIL-125(Ti) catalyst with reusability up to three runs. The heterogeneous titanium-terephthalate metal organic framework catalyst can overcome the disadvantages of traditional homogeneous Fenton catalyst. The results indicate that NH<sub>2</sub>-MIL-125(Ti) can be a new material for Fenton-like oxidation processes.



UMS  
UNIVERSITI MALAYSIA SABAH

## ABSTRAK

### **PEMANGKIN PENGOKSIDAAN HETEROGEN BAGI METILENA BIRU MELALUI KERANGKA ORGANIK LOGAM BERFUNGSIAN-AMINA TITANIUM TEREFTALAT, NH<sub>2</sub>-MIL-125(Ti)**

Pembentukan enapcemar ferum oksida, kebergantungan kepada pH dan guna semula pemangkin yang lemah merupakan beberapa kesusahan reagen Fenton yang ketara. Dalam kajian ini, kompaun logam-organik titanium-tereftalat, NH<sub>2</sub>-MIL-125(Ti), telah dicadangkan sebagai pemangkin heterogen "Fenton-like" untuk degradasi metilena biru. NH<sub>2</sub>-MIL-125(Ti) adalah satu sebatian logam-organik yang mempunyai luas permukaan yang tinggi, sifat-sifat fotomangkin dan juga dua jenis liang yang unik. MIL-125(Ti) dan juga NH<sub>2</sub>-MIL-125(Ti) telah disediakan melalui kaedah reflux dan diaktifkan dengan kaedah pertukaran pelarut konvensional. Kedua-dua sample tersebut telah pencirian melalui XRD dan FTIR. SEM imej telah menunjukkan bahawa NH<sub>2</sub>-MIL-125(Ti) mempunyai morfologi sfera dengan saiz di antara 250 nm ke 500 nm, di mana ia adalah lebih kurang separuh dari saiz MIL-125(Ti). NH<sub>2</sub>-MIL-125(Ti) juga menunjukkan kestabilan yang tinggi di dalam air sehingga 24 jam. Apabila cahaya visible dan UV-A digunakan, aktiviti penjerapan dan fotoaktif yang tinggi telah diperhatikan. Di samping itu, NH<sub>2</sub>-MIL-125(Ti) telah dibuktikan sebagai suatu pemangkin "Fenton-like" yang bukan-ferum yang cekap. Kesan sinergi telah diperhatikan di antara NH<sub>2</sub>-MIL-125(Ti) dan H<sub>2</sub>O<sub>2</sub>, dengan penyingkiran dan penguraian 40 ppm metilena biru sehingga 84 %. Keputusan telah menunjukkan bahawa, dalam sistem pemangkin NH<sub>2</sub>-MIL-125(Ti)/ H<sub>2</sub>O<sub>2</sub>, •OH dan h<sup>+</sup> merupakan spesies yang dominan dalam oksidasi "Fenton-like". Peningkatan-foto telah dibuktikan berkesan di mana 92 % penyingkiran telah dicapai apabila cahaya UV-A telah digunakan. NH<sub>2</sub>-MIL-125(Ti) telah mempunyai pergantungan kepada pH yang rendah di mana penguraian yang stabil boleh dicapai di antara pH 3 hingga 9. Larut lesap titanium yang amat rendah telah dikesan menunjukkan NH<sub>2</sub>-MIL-125(Ti) mempunyai stabiliti yang tinggi serta penggunaan semula sehingga tiga kali. Oleh itu pemangkin sebatian logam-organik heterogen boleh mengatasi kelemahan-kelemahan pemangkin homogen "Fenton" yang tradisional. Keputusan yang didapati telah menunjukkan bahawa NH<sub>2</sub>-MIL-125(Ti) merupakan satu bahan yang baru didalam proses oksidasi "Fenton-like".

## TABLE OF CONTENTS

	Page
<b>TITLE</b>	i
<b>DECLARATION</b>	ii
<b>CERTIFICATION</b>	iii
<b>ACKNOWLEDGEMENTS</b>	iv
<b>ABSTRACT</b>	v
<b><i>ABSTRAK</i></b>	vi
<b>TABLE OF CONTENTS</b>	vii
<b>LIST OF TABLES</b>	xi
<b>LIST OF FIGURES</b>	xii
<b>LIST OF SYMBOLS AND ABBREVIATIONS</b>	xviii
<b>LIST OF APPENDICES</b>	xxi
<b>CHAPTER 1: INTRODUCTION</b>	1
1.1 Fenton-catalyzed Reaction	1
1.2 Limitations of Fenton-catalyzed Processes	2
1.3 Modified Fenton Processes	2
1.4 MOF-based Fenton Catalysts	3
1.5 MIL-125(Ti) and NH <sub>2</sub> -MIL-125(Ti)	4
1.6 Objectives	5
1.7 Scope of study	5
<b>CHAPTER 2: LITERATURE REVIEW</b>	6
2.1 Advanced Oxidation Processes (AOPs)	6
2.2 Fenton-catalyzed Processes	8
2.3 Fundamental Fenton Chemistry	9

2.4	Specifications and Limitations of Fenton-catalyzed Processes	11
2.5	Modified Fenton Processes	13
2.5.1	Chelated Forms Fenton Catalysts	14
2.5.2	Photo-Fenton Process	14
2.5.3	Electro-Fenton Process	17
2.5.4	Sono-Fenton Process	18
2.5.5	Combined Modified-Fenton Process	19
2.5.6	Heterogeneous Fenton Catalysts	20
2.5.7	Non-Ferrous Fenton Catalysts	22
2.5.8	MOF-based Fenton Catalysts	23
2.6	Nanoporous Materials	25
2.7	Metal–Organic Frameworks (MOFs)	26
2.8	MIL-125(Ti) and NH <sub>2</sub> -MIL-125(Ti)	30
2.9	Applications of MIL-125(Ti) and NH <sub>2</sub> -MIL-125(Ti)	36
2.10	Modifications of MIL-125(Ti) and NH <sub>2</sub> -MIL-125(Ti)	39
2.10.1	Organic Linker Modifications	39
2.10.2	Metal Nanoparticles Fabrication	40
2.10.3	Semiconductor Coupling	42
2.10.4	MOFs-Derived TiO <sub>2</sub>	43
2.11	Potential Application of Titanium-based MOFs as Fenton Catalyst	43
2.12	Methylene Blue	44
	<b>CHAPTER 3: METHODOLOGY</b>	46
3.1	Materials	46
3.2	Experimental Flow Chart	46
3.3	Preparation of MIL-125(Ti)-type Materials	48



3.3.1	Synthesis of MIL-125(Ti)	48
3.3.2	Synthesis of NH <sub>2</sub> -MIL-125(Ti)	49
3.4	Characterization	49
3.4.1	Identification of the Samples	49
3.4.2	Morphology of the Samples	50
3.4.3	Identification of Surface Functional Groups of Samples	51
3.4.4	Optical Absorption Properties of Samples	52
3.4.5	Water Stability Test	53
3.5	Adsorption Studies	53
3.6	Photocatalytic Degradation Studies	54
3.7	Fenton-Like Behavior Studies	54
3.7.1	Effect of Light Sources	55
3.7.2	Effect of Initial Concentrations of H <sub>2</sub> O <sub>2</sub>	55
3.7.3	Effect of Time Duration	55
3.7.4	Effect of Initial pH	55
3.7.5	Catalyst Recoverability and Reusability	56
3.7.6	Mechanism Studies	57
3.7.7	Sequence of H <sub>2</sub> O <sub>2</sub> Addition	58
<b>CHAPTER 4: RESULTS AND DISCUSSION</b>		<b>59</b>
4.1	Synthesis of MIL-125(Ti) and NH <sub>2</sub> -MIL-125(Ti)	59
4.2	Identification of The Samples	62
4.3	Crystal Morphology of the Samples	63
4.4	Identification of Surface Functional Group of Samples	65
4.5	Optical Absorption Properties of Samples	67
4.6	Water Stability Test	68

4.7	Adsorption Studies	72
4.8	Photocatalytic Degradation Studies	73
4.9	Fenton-Like Behavior Studies	75
4.9.1	Effect of Light Sources	76
4.9.2	Comparison of Different Systems	77
4.9.3	Effect of Initial Concentration of H <sub>2</sub> O <sub>2</sub>	81
4.9.4	Effect of Time Duration	86
4.9.5	Effect of Initial pH	90
4.9.6	Catalyst Recoverability and Reusability	95
4.9.7	Mechanism Studies	98
4.9.8	Sequence of H <sub>2</sub> O <sub>2</sub> Addition	102
4.9.9	Comparison of Different Fenton Catalysts	105
<b>CHAPTER 5: CONCLUSIONS AND RECOMMENDATIONS</b>		107
5.1	Conclusion	107
5.2	Recommendations	108
<b>REFERENCES</b>		110
<b>APPENDICES</b>		133

## LIST OF TABLES

	Page
Table 2.1: Common combination of AOPs	7
Table 2.2: Types of Modified Fenton Processes	13
Table 2.3: Classification of porous materials by pore size	26
Table 4.1: Pseudo-first-order kinetics and half-life for different processes	81
Table 4.2: Reaction rate constants value of MB degradation by NH <sub>2</sub> -MIL-125(Ti)/H <sub>2</sub> O <sub>2</sub> under different condition	86
Table 4.3: Pseudo-first-order kinetics, R <sub>2</sub> and k values of Fenton-like reactions under 2 and 4 hours duration	88
Table 4.4: Calculated R <sub>2</sub> , rate constants and half-life of pseudo-first-order kinetics of NH <sub>2</sub> -MIL-125(Ti)/H <sub>2</sub> O <sub>2</sub> under different pH values	94
Table 4.5: Titanium content of treated MB solutions by NH <sub>2</sub> -MIL-125(Ti)/H <sub>2</sub> O <sub>2</sub> system under different pH conditions	97
Table 4.6: Comparison of MB degradation by different Fenton-based or MIL-125(Ti)-based catalyst	106

## LIST OF FIGURES

	Page
Figure 2.1: Classification of MOFs	28
Figure 2.2: Cyclic octamers (SBU-8) of edge- and corner-sharing $\text{TiO}_5(\text{OH})$ octahedral SBUs	30
Figure 2.3: Terephthalate ligand (BDC)	31
Figure 2.4: A schematic structure of MIL-125(Ti)	31
Figure 2.5: A cyclic octamer linked by 12 BDC ligands to form a body-centered cubic packing	32
Figure 2.6: Pore structure of MIL-125(Ti) with octahedral cage (blue) and tetrahedral cage (green)	32
Figure 2.7: Pore network of MIL-125 viewed from [001] direction	33
Figure 2.8: [010] orientation of MIL-125	33
Figure 2.9: 2-amino-terephthalate ligand ( $\text{NH}_2$ -BDC)	34
Figure 2.10: The view of crystal structure of X-MIL-125(Ti) form [100] direction. Red ball or X represent H in MIL-125(Ti), while in the case of $\text{NH}_2$ -MIL-125(Ti) is $\text{NH}_2$ group	34
Figure 2.11: MIL-125(Ti) crystal structure	35
Figure 2.12: $\text{NH}_2$ -MIL-125(Ti) crystal structure	36
Figure 2.13: 2,3,5,6-tetramethylterephthalate ligand ( $(\text{CH}_3)_4$ -BDC)	39
Figure 2.14: Post-synthesis modified (PSM) methyl-red terephthalate linker	40
Figure 2.15: 2,5-diaminoterephthalate ( $(\text{NH}_2)_2$ -BDC) linker	40
Figure 2.16: Methylene blue	44

Figure 3.1:	Experimental flow chart	47
Figure 3.2:	Schematic diagram of heating process of mixture of H <sub>2</sub> BDC and DMF	48
Figure 3.3:	Schematic diagram of reflux setup	49
Figure 3.4:	X-ray diffractometer (PHILIPS X'PERT PRO PW 3040)	50
Figure 3.5:	Scanning electron microscope (JEOL JSM-5610LV)	51
Figure 3.6:	FTIR Analysis Instrument (Perkin Elmer, Spectrum 100)	52
Figure 3.7:	UV-Vis Spectrophotometer (Thermo Scientific, Evolution 220)	52
Figure 3.8:	UV-Vis spectrophotometer (Agilent Cary 60)	53
Figure 3.9:	Setup for the experiment	54
Figure 3.10:	pH meter (EUTECH, pH 700)	56
Figure 3.11:	Inductively coupled plasma optical emission spectrometer (Perkin Elmer Optima 5300 DV)	57
Figure 4.1:	H <sub>2</sub> BDC and DMF mixture	59
Figure 4.2:	NH <sub>2</sub> -H <sub>2</sub> BDC and DMF mixture	60
Figure 4.3:	MIL-125(Ti) precursor	60
Figure 4.4:	NH <sub>2</sub> -MIL-125(Ti) precursor	61
Figure 4.5:	MIL-125(Ti) powder	61
Figure 4.6:	NH <sub>2</sub> -MIL-125(Ti) powder	62
Figure 4.7:	XRD pattern of (a) anatase TiO <sub>2</sub> ; (b) rutile TiO <sub>2</sub> ; (c) simulated MIL-125(Ti); (d) as-prepared MIL-125(Ti) and (e) as-prepared NH <sub>2</sub> -MIL-125(Ti)	63
Figure 4.8:	SEM images of MIL-125(Ti) in 5000x magnification	64

Figure 4.9:	SEM images of MIL-125(Ti) in 10000x magnification	64
Figure 4.10:	SEM images of NH <sub>2</sub> -MIL-125(Ti) in 5000x magnification	65
Figure 4.11:	SEM images of NH <sub>2</sub> -MIL-125(Ti) in 10000x magnification	65
Figure 4.12:	FTIR spectrum of (a) MIL-125(Ti) and (b) NH <sub>2</sub> -MIL-125(Ti)	66
Figure 4.13:	UV-Vis spectrum of MIL-125(Ti) and NH <sub>2</sub> -MIL-125(Ti)	67
Figure 4.14:	Plot of $(\alpha h\nu)^2$ versus photon energy ( $h\nu$ ) of MIL-125(Ti) and NH <sub>2</sub> -MIL-125(Ti)	68
Figure 4.15:	XRD pattern of (a) MIL-125(Ti) fresh sample; (b) MIL-125(Ti) and (c) NH <sub>2</sub> -MIL-125(Ti) after water dispersion for 4 hours	69
Figure 4.16:	XRD pattern of (a) MIL-125(Ti) fresh sample; after water dispersion for (b) 1 hour; (c) 2 hours; (d) 4 hours and (e) H <sub>2</sub> BDC	70
Figure 4.17:	XRD pattern of (a) NH <sub>2</sub> -MIL-125(Ti) fresh sample; after water dispersion for (b) 4 hours; (c) 12 hours; (d) 24 hours and (e) NH <sub>2</sub> -H <sub>2</sub> BDC	71
Figure 4.18:	MB adsorption performance of NH <sub>2</sub> -MIL-125(Ti) at different catalyst dosage	73
Figure 4.19:	Photocatalytic performance of 0.075 g/L of NH <sub>2</sub> -MIL-125(Ti) on degradation of 40 ppm MB using visible and UV-A irradiation	74
Figure 4.20:	MB degradation of H <sub>2</sub> O <sub>2</sub> and NH <sub>2</sub> -MIL-125(Ti) in dark condition	75
Figure 4.21:	MB degradation of H <sub>2</sub> O <sub>2</sub> and NH <sub>2</sub> -MIL-125(Ti) under visible light irradiation	76
Figure 4.22:	MB degradation of H <sub>2</sub> O <sub>2</sub> and NH <sub>2</sub> -MIL-125(Ti) under UV-A light irradiation	77

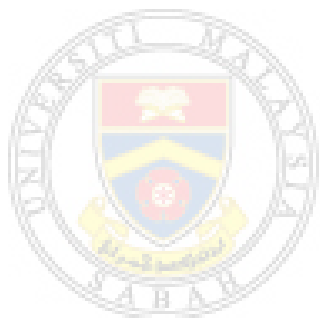
Figure 4.23:	Degradation of MB by different combinations of oxidant, catalyst and light irradiation	78
Figure 4.24:	Pseudo-first-order kinetics curves of MB degradation by different systems	80
Figure 4.25:	Apparent reaction rate constants of MB degradation by different systems	81
Figure 4.26:	Degradation of MB by NH <sub>2</sub> -MIL-125(Ti) with different initial concentration of H <sub>2</sub> O <sub>2</sub> in dark condition	82
Figure 4.27:	Apparent reaction rate constants of MB degradation by NH <sub>2</sub> -MIL-125(Ti) with different initial concentration of H <sub>2</sub> O <sub>2</sub> in dark condition	83
Figure 4.28:	Degradation of MB by NH <sub>2</sub> -MIL-125(Ti) with different initial concentration of H <sub>2</sub> O <sub>2</sub> under visible irradiation	84
Figure 4.29:	Apparent reaction rate constants of MB degradation by NH <sub>2</sub> -MIL-125(Ti) with different initial concentration of H <sub>2</sub> O <sub>2</sub> with visible light irradiation	84
Figure 4.30:	Degradation of MB by NH <sub>2</sub> -MIL-125(Ti) with different initial concentration of H <sub>2</sub> O <sub>2</sub> under UV-A irradiation	85
Figure 4.31:	Apparent reaction rate constants of MB degradation by NH <sub>2</sub> -MIL-125(Ti) with different initial concentration of H <sub>2</sub> O <sub>2</sub> with UV-A irradiation	86
Figure 4.32:	Degradation of MB by NH <sub>2</sub> -MIL-125(Ti)/H <sub>2</sub> O <sub>2</sub> under dark condition and with light irradiation	87
Figure 4.33:	Pseudo-first-order kinetics curves of MB degradation with prolonged reaction time	88
Figure 4.34:	Degradation efficiency of MB by NH <sub>2</sub> -MIL-125(Ti) with addition of H <sub>2</sub> O <sub>2</sub> once (straight line) and twice (dotted line)	89

Figure 4.35:	The initial pH value of unadjusted MB solution	90
Figure 4.36:	The pH value of MB solution after adjusted with 0.1 M $\text{H}_2\text{SO}_4$ solution	90
Figure 4.37:	The MB solution was adjusted to near neutral condition with 0.1 M NaOH solution	91
Figure 4.38:	The pH value of MB solution was adjusted alkaline condition with 0.1 M NaOH solution	91
Figure 4.39:	The adsorption and photocatalytic degradation of MB solutions under different pH conditions	92
Figure 4.40:	Photocatalytic degradation performance of MB solutions by $\text{NH}_2\text{-MIL-125(Ti)/H}_2\text{O}_2$ with different initial pH value	93
Figure 4.41:	Pseudo-first-order kinetics curves of MB degradation under different initial pH values	94
Figure 4.42:	Cycling runs of MB degradation over $\text{NH}_2\text{-MIL-125(Ti)/H}_2\text{O}_2$	96
Figure 4.43:	Degradation of treated MB solution with $\text{H}_2\text{O}_2$ oxidant and no catalyst	97
Figure 4.44:	Degradation of MB by $\text{NH}_2\text{-MIL-125(Ti)/H}_2\text{O}_2$ with different scavengers in dark condition	99
Figure 4.45:	Degradation of MB by $\text{NH}_2\text{-MIL-125(Ti)/H}_2\text{O}_2$ with different scavengers in visible irradiation	100
Figure 4.46:	Degradation of MB by $\text{NH}_2\text{-MIL-125(Ti)/H}_2\text{O}_2$ with different scavengers in UV-A irradiation	100
Figure 4.47:	Degradation efficiencies of MB by $\text{NH}_2\text{-MIL-125(Ti)/H}_2\text{O}_2$ with different scavengers	101
Figure 4.48:	Electron-hole separation of excited-state $\text{NH}_2\text{-MIL-125(Ti)}$	101
Figure 4.49:	Schematic diagram of proposed mechanism of Fenton-like	102



activation of  $H_2O_2$  by  $NH_2$ -MIL-125(Ti)

- Figure 4.50: Degradation of MB by  $NH_2$ -MIL-125(Ti)/ $H_2O_2$  system under different  $H_2O_2$  addition sequences 103
- Figure 4.51: Schematic diagram of active sites blockage effect in  $NH_2$ -MIL-125(Ti) by MB molecules. 104
- Figure 4.52: Schematic diagram of reaction mechanism of adsorption and Fenton-like process by  $NH_2$ -MIL-125(Ti)/ $H_2O_2$  system 104



UMS  
UNIVERSITI MALAYSIA SABAH

## LIST OF SYMBOLS AND ABBREVIATIONS

$(\text{CH}_3)_4\text{-BDC}$	2,3,5,6-tetramethylterephthalate Linker
$(\text{NH}_2)_2\text{-BDC}$	2,5-diaminoterephthalate Linker
$\epsilon$	Porosity
$\bullet\text{OH}$	Hydroxyl Radical
$\alpha$	Adsorption Coefficient
$\alpha\text{-Fe}_2\text{O}_3$	Hematite
$\alpha\text{-FeOOH}$	Goethite
$\gamma\text{-Fe}_2\text{O}_3$	Maghemite
$\lambda$	Wavelength
$\lambda_{\text{max}}$	Maximum Absorbance Wavelength
2D	2-dimensional Coordination Network
3D	3-dimensional Coordination Network
$\text{Al}^0$	Zero-valent Aluminium
AOPs	Advance Oxidation Processes
BDC	Terephthalate Linker
$\text{BiFeO}_3$	Bismuth Ferrite
$c$	speed of light
$\text{C}_2\text{O}_4^{\bullet-}$	Oxalyl Radical Anions
$C_i$	Concentration at Time t
$C_0$	Initial Concentration
CB	Conduction Band
DFT	Density Functional Theory
DOE	Department of Environment
DR UV-Vis	Diffuse Reflectance UV-Visible Spectrophotometer
$e^-$	Electron

$E_g$	Energy Band Gap
$Fe^0$	Nanoscale Zero-Valent Iron Particles
$Fe_3O_4$	Magnetite
Fe(II)	Ferrous Ion
Fe(III)	Ferric Ion
$Fe(OH)^{2+}$	Aquated Fe(III) Species
$Fe-OOH^{2+}$	Fe(III)-peroxide
FTIR	Fourier Transform Infrared Spectroscopy
$g-C_3N_4$	Graphite-like Carbon Nitride
$h^+$	Hole
$H_2BDC$	Terephthalic Acid
$H_2O_2$	Hydrogen Peroxide
$HO_2\bullet$	Hydroperoxyl Radical
$HSO_5^-$	Peroxymonosulfate
$h$	Planck Constant
$h\nu$	Photon Energy
ICP-OES	Inductively Coupled Plasma Optical Emission Spectrometer
IRMOF	Isoreticular MOFs
IUPAC	International Union of Pure and Applied Chemistry
$k$	Reaction Rate Constant
LCCT	Ligand-to-Cluster Charge Transfer
LMCT	Ligand-to-Metal Charge Transfer
MB	Methylene Blue
MIL	Materials of Institut Lavoisier
MIL-125(Ti)	Titanium (IV) Dicarboxylate
MOF	Metal Organic Framework
MOFs	Metal Organic Frameworks

MY	Metanil Yellow
NH <sub>2</sub> -BDC	2-aminoterephthalate Linker
NH <sub>2</sub> -H <sub>2</sub> BDC	2-aminoterephthalic Acid
NH <sub>2</sub> -MIL-125(Ti)	Amine-functionalized Titanium (IV) Dicarboxylate
NPs	Nanoparticles
O <sub>2</sub> <sup>-•</sup>	Superoxide Anion
PCPs	Porous Coordination Polymers
PEF	Photo-Electro-Fenton Process
POMs	Polyoxometalates
PSM	Post-Synthesis Modified
R-CO <sub>2</sub> -Fe <sup>3+</sup>	Fe(III)-polycarboxylate
R•	Carbon-centered Radical
R <sup>2</sup>	Correlation Coefficient
rGO	Reduced Graphene Oxide
RhB	Rhodamine B
RR195	Reactive Red Dye 195
S <sub>2</sub> O <sub>8</sub> <sup>2-</sup>	Persulfate
SBU-8	Cyclic Octamers
SBU <sub>s</sub>	Secondary Building Units
SEF	Sono-Electro-Fenton Process
SEM	Scanning Electron Microscope
SPEF	Solar-Photo-Electro-Fenton
SPF	Sono-Photo-Fenton Process
t <sub>1/2</sub>	Half-life
UV-Vis	UV-Visible Spectrophotometer
XRD	X-Ray Diffraction
WHO	World Health Organization

## LIST OF APPENDICES

	Page	
Appendix A	Calibration Curve of Methylene Blue Dye Solution	133
Appendix B	Pseudo-First-Order Kinetics of Different Concentration of $H_2O_2$ in Dark Condition	135
Appendix C	Pseudo-First-Order Kinetics of Different Concentration of $H_2O_2$ in Visible Irradiation	136
Appendix D	Pseudo-First-Order Kinetics of Different Concentration of $H_2O_2$ in UV-A Irradiation	137
Appendix E	Detection of trace metals in treated MB solution by ICP-OES	138



UMS  
UNIVERSITI MALAYSIA SABAH

# CHAPTER 1

## INTRODUCTION

### 1.1 Fenton-catalyzed Processes

Over the past few decades, advanced oxidation processes (AOPs) have gained in popularity as one of the clean approaches in pollution control (Wang, 2008). AOPs often recognized as superior to other treatment methods because of its destructive nature that can lead to almost complete mineralization in wide range of pollutants (Ai *et al.*, 2014; Dutta *et al.*, 2001; Stasinakis, 2008). AOPs mechanism involves in-situ generation of highly reactive radicals which attack pollutants rapidly and non-selectively into less harmful substances that can be further biodegraded or, in some instance, decomposed into water and carbon dioxide (Contreras *et al.*, 2002).

Generally, AOPs utilizes a combination of powerful oxidants with catalysts and/or irradiation (Stasinakis, 2008).  $\text{H}_2\text{O}_2$  is one of the common oxidants which frequently used in AOPs (Ai *et al.*, 2014). Hydrogen peroxide ( $\text{H}_2\text{O}_2$ ) is highly active oxidant with only water as a sole by-product (Lei *et al.*, 2005). As an environmentally benign oxidant, it is also inexpensive and safer to use than organic peroxides or peracids (Saedi *et al.*, 2012).  $\text{H}_2\text{O}_2$  by itself however, is insufficient. Activation of  $\text{H}_2\text{O}_2$  by transition metals, semiconductor, UV light or ultra-sonication is required to promote  $\text{H}_2\text{O}_2$  decomposition into hydroxyl radicals ( $\bullet\text{OH}$ ) (Ai *et al.*, 2014; Dionysiou *et al.*, 2000; Lei *et al.*, 2005).

Fenton's reagent has attracted increasing attention in the activation of  $\text{H}_2\text{O}_2$  since its discovery a century ago (Neyens and Baeyens, 2003). It refers to the redox reaction between ferrous [ $\text{Fe(II)}$ ] ion and  $\text{H}_2\text{O}_2$  which lead to the formation of powerful oxidants which includes  $\bullet\text{OH}$  (Pignatello, Oliveros, and MacKay, 2006; Stasinakis, 2008). With in-situ generation of highly reactive radicals, Fenton-catalyzed reaction has been proven to be an effective treatment in many organic

pollutants including aromatic compounds, phenols, chlorine-containing compounds, formaldehyde and synthetic dyes (Dutta *et al.*, 2001).

## **1.2 Limitations of Fenton-catalyzed Processes**

Fenton-catalyzed treatment is an established practice with high effectiveness and low energy consumption (Bauer and Fallmann, 1997; Contreras *et al.*, 2002; Wang, 2008). Also, Fenton's reagent is more economic when compared to other AOPs which required O<sub>3</sub> or UV (Wang, 2008). Nonetheless, this approach is not without its drawbacks. Some of the drawbacks encountered include iron oxide sludge formation, pH limitations, large amount of reagents needed, sophisticated system required for catalyst-product separation process, poor catalyst reusability and recoverability (Dutta *et al.*, 2001; Munter, 2001; Ramirez *et al.*, 2007; Saedi *et al.*, 2012; Strlič *et al.*, 2003). As a result, many researchers are looking for new catalyst able to activate H<sub>2</sub>O<sub>2</sub> while overcoming the critical drawbacks such as modification of current Fenton processes or utilization of other non-iron based materials with Fenton properties.

## **1.3 Modified Fenton Processes**

Throughout the years, different approaches have been made to develop a more efficient Fenton catalyst. Some approaches have proven to be effective in expanding the effective pH range of Fenton reactions and prevent the sludge formation. These modifications including immobilizes of iron on materials, forms iron complexes with chelating agents and utilizes heterogeneous Fenton catalyst such as solid iron compounds and inorganic iron minerals (Babuponnusami and Muthukumar, 2014; Pignatello, Oliveros, and MacKay, 2006). However, the modified Fenton catalyst largely reduced its accessible surface active sites hence causing a decline in its catalytic activity (Pignatello, Oliveros, and MacKay, 2006). Also, instability of heterogeneous Fenton catalyst can cause iron leaching during the process which makes the reaction mainly homogeneous and leads to poor catalyst reusability (Babuponnusami and Muthukumar, 2014; Hartmann, Kullmann, and Keller, 2010).

Irradiation is another common method to improve the effectiveness of Fenton reactions. By utilizing light irradiation and sonication, enhancement can be observed in most cases in Fenton reactions. Photo-Fenton process and sono-Fenton process both can increase the rates of regeneration of Fe(II) ions (Equation 2.2 and 2.3) and reactions between Fe(II) ions and H<sub>2</sub>O<sub>2</sub> (Equation 2.1). To reduce the amount of reagent required for the reactions, Fenton process can also combine with electrochemical reactions to in-situ generate Fe ions or/and H<sub>2</sub>O<sub>2</sub> oxidants which is commonly known as electro-Fenton process (Pignatello, Oliveros, and MacKay, 2006).

According the Department of Environment (DOE) Malaysia directive, the discharge limit of iron content in industrial effluent is only range from 1 to 5 ppm. Therefore, in homogeneous Fenton reactions where 50 to 80 ppm of ferrous ions is normally required, sophisticated system for catalyst-product separation process is needed (Department of Environment, 2010; Hartmann, Kullmann, and Keller, 2010). To overcome the problems, researchers have expanded their studies to non-ferrous Fenton catalysts. Many metal ions and its complex forms have been identified as potential candidates such as aluminum (Al), chromium (Cr), copper (Cu), manganese (Mn), ruthenium (Ru) and cerium (Ce). The mixtures of these metal compounds with H<sub>2</sub>O<sub>2</sub> were named "Fenton-like" reagents (Bokare and Choi, 2014; Goldstein, Meyerstein, and Czapski, 1993).

#### **1.4 MOF-based Fenton Catalysts**

Many researchers have been studying the effects of metal-organic frameworks (MOFs) and H<sub>2</sub>O<sub>2</sub> as a co-dependent system aiming to increase catalytic performance. MOFs are hybrid materials which connect metal-ion clusters with multitopic ligands forming a three-dimensional network with a molecular-defined porosity (Wang *et al.*, 2015). Many researchers consider MOFs to be superior to other porous coordination polymers (PCPs) in terms of internal surface area, micropore volume, tunable properties and functionalities (Ai *et al.*, 2014; Jeremias *et al.*, 2013; Li *et al.*, 2017). Previous studies have shown that Fenton-like behavior is found in a number of iron-based MOFs like Fe-bpydc, MIL-100(Fe), NH<sub>2</sub>-MIL-88B(Fe), MIL-53(Fe) and MIL-101(Fe) (Ai *et al.*, 2014; Li *et al.*, 2017; Li *et al.*, 2016;